THE JOURNAL OF BIOLOGICAL CHEMISTRY
Vol. 277, No. 28, Issue of July 12, pp. 25537–25544, 2002
Printed in U.S.A.

Structure of Human Chitotriosidase

IMPLICATIONS FOR SPECIFIC INHIBITOR DESIGN AND FUNCTION OF MAMMALIAN CHITINASE-LIKE LECTINS*

Received for publication, February 18, 2002, and in revised form, April 16, 2002
Published, JBC Papers in Press, April 17, 2002, DOI 10.1074/jbc.M201636200

Fabrizia Fusetti‡, Holger von Moeller§, Douglas Houston§, Henriëtte J. Rozeboom‡, Bauke W. Dijkstra‡, Rolf G. Boot¶, Johannes M. F. G. Aerts¶, and Daan M. F. van Aalten§‖

From the ‡Laboratory of Biophysical Chemistry, University of Groningen, 9747 AG Groningen, The Netherlands, §Wellcome Trust Biocentre, School of Life Sciences, University of Dundee, Dundee DD1 5EH, Scotland, United Kingdom, and ¶University of Amsterdam, Academic Medical Centre, Dept. of Biochemistry, 1105 AZ, Amsterdam, The Netherlands

Chitin hydrolases have been identified in a variety of organisms ranging from bacteria to eukaryotes. They have been proposed to be possible targets for the design of novel chemotherapeutics against human pathogens such as fungi and protozoan parasites as mammals were not thought to possess chitin-processing enzymes. Recently, a human chitotriosidase was described as a marker for Gaucher disease with plasma levels of the enzyme elevated up to 2 orders of magnitude. The chitotriosidase was shown to be active against colloidal chitin and is inhibited by the family 18 chitinase inhibitor allosamidin. Here, the crystal structure of the human chitotriosidase and complexes with a chitooligosaccharide and allosamidin are described. The structures reveal an elongated active site cleft, compatible with the binding of long chitin polymers, and explain the inactivation of the enzyme through an inherited genetic deficiency. Comparison with YM1 and HCgp-39 shows how the chitinase has evolved into these mammalian lectins by the mutation of key residues in the active site, tuning the substrate binding specificity. The soaking experiments with allosamidin and chitooligosaccharides give insight into ligand binding properties and allow the evaluation of differential binding and design of species-selective chitinase inhibitors.

Family 18 chitinases hydrolyze chitin, an abundant polymer of *N*-acetylglucosamine (NAG).[1] These enzymes have been identified in bacteria (1), fungi (2), insects (3), plants (4), viruses (5), and protozoan parasites (6). Humans were thought not to possess or process chitin, and therefore chitinases have been proposed to be targets for the development of inhibitors with chemotherapeutical potential as insecticides, fungicides, and antimalarials (6–9). Recently, however, it was discovered that humans have a chitinase activity that was found to be elevated up to 2 orders of magnitude in the plasma of patients suffering from Gaucher disease, a rare genetic disorder that is caused by a mutation in the glucocerebrosidase gene (10, 11). Purification of this activity from a Gaucher spleen revealed that, although transcribed from a single gene, the enzyme occurs in two major forms of 39 and 50 kDa. The subsequent cloning of its cDNA from a macrophage library showed that the 50-kDa form can be converted to the 39-kDa form post-translationally or by RNA processing (12–15). The enzyme is able to cleave chitotriose (and was termed chitotriosidase) but also hydrolyzes colloidal chitin to yield chitobiose and is thus thought to be an exochitinase (12, 16). Although the 39-kDa form is sufficient for the chitinolytic activity, the additional C-terminal domain has been shown to play a role in processing colloidal chitin and has been proposed to be a chitin binding domain, similar to other domains observed in the structures of chitinase A/B from *Serratia marcescens* (14, 17, 18). The chitotriosidase gene appears not to be essential, as about 35% of humans are heterozygous (6% homozygous) for an inactivated form of the gene (11, 15).

Although the enzyme has been characterized in detail, its function has not been fully defined. The observations that it is able to degrade both colloidal chitin and chitin in the cell wall of the fungal pathogen *Candida albicans* have prompted the hypothesis that the chitotriosidase plays a role in defense against chitinous human pathogens (15, 16). Indirect support for this hypothesis has recently come from a study showing that humans deficient in chitotriosidase activity are more susceptible to nematodal infections (19). Parasitic nematodes synthesize chitin during several stages of their lifecycle, and a human chitotriosidase could interfere with these processes. Thus, although the chitotriosidase is not essential from a general metabolic point of view, it may play a key role as a pathogen-defense protein. This implies that although chitinases in the pathogenic organisms themselves may be targets for the design of small molecule inhibitors with chemotherapeutical potential, it would be beneficial to exclude inhibitors that show strong activity against the human chitotriosidase. The most potent inhibitor currently known, the pseudotrisaccharide allosamidin (3), inhibits all family 18 chitinases with K_i values in the nanomolar to micromolar range, the human enzyme being inhibited at a K_i of 0.4 μM (16).

Here, we describe the crystal structures of human chitotriosidase in two crystal forms (at 2.35- and 2.1-Å resolution), a complex with chitobiose, and a soaking experiment with allosamidin. The chitotriosidase structure provides insight into the molecular basis of the inherited genetic inactivation of the enzyme and the evolution of the chitinase to form a structural

* The costs of publication of this article were defrayed in part by the payment of page charges. This article must therefore be hereby marked "*advertisement*" in accordance with 18 U.S.C. Section 1734 solely to indicate this fact.

The atomic coordinates and structure factors (code 1GUV, 1LG1, 1LG2) have been deposited in the Protein Data Bank, Research Collaboratory for Structural Bioinformatics, Rutgers University, New Brunswick, NJ (http://www.rcsb.org/).

‖ Supported by a Wellcome Trust Career Development Research Fellowship. To whom correspondence should be addressed. Fax: 44-1382-345764; E-mail: dava@davapc1.bioch.dundee.ac.uk.

[1] The abbreviations used are: NAG, *N*-acetylglucosamine; ChiA, chitinase A; ChiB, chitinase B; CAPS, 3-(cyclohexylamino)propanesulfonic acid.

TABLE I
Details of data collection and structure refinement for native chitotriosidase and complexes
Values between brackets are for the highest resolution shell. All measured data were included in structure refinement.

	Native I	Native II	NAG_5	Allosamidin
Space group	$P4_32_12$	$P2_1$	$P4_32_12$	$P4_32_12$
Cell dimensions (Å)	$a = 93.26$	$a = 45.17$	$a = 94.40$	$a = 98.37$
	$b = 93.26$	$b = 47.29$	$b = 94.40$	$b = 98.37$
	$c = 89.80$	$\beta = 102.6°$, $c = 84.73$	$c = 87.98$	$c = 88.15$
Resolution range (Å)	17–2.35	13.4–2.1	35–2.78	30–2.7
	(2.43–2.35)	(2.15–2.1)	(2.88–2.78)	(2.8–2.7)
No. observed reflections	95454 (9001)	73055 (4290)	56839 (4190)	35543 (3335)
No. unique reflections	17192 (1670)	20533 (1330)	10485 (916)	11398 (1104)
Redundancy	5.6 (5.4)	3.6 (3.2)	5.4 (4.6)	3.1 (3.0)
I/σI	11.1 (3.9)	14.3 (4.6)	15.0 (3.4)	6.3 (2.4)
Completeness (%)	99.8 (99.9)	99.6 (97.0)	97.8 (87.2)	98.5 (98.1)
R_{merge} (%)	8.3 (55.3)	7.2 (22.5)	10.6 (45.5)	12.1 (37.2)
R_{cryst} (%)	21.6	20.4	19.7	
R_{free} (%)	26.2	22.7	26.9	
No. R_{free}reflections	545	2077	1042	
No. protein atoms	2820	2797	2864	
No. water molecules	273	201	17	
Refined carbohydrate	none	none	NAG_2	
R. M. S. deviations from ideal geometry:				
bonds (Å)	0.009	0.005	0.007	
angles (°)	1.4	1.2	1.2	
$<B_{prot}>$ (Å^2)	37.8	19.1	48.5	
$<B_{carbohydrate}>$ (Å^2)			48.8	

scaffold for several mammalian lectins. By comparison of the active site with that of chitinases from pathogenic organisms, we show that it should be possible to design allosamidin derivatives or other small molecules that are selective inhibitors.

MATERIALS AND METHODS

Purification and Crystallization—Human recombinant chitotriosidase was purified from the medium of stably transfected baby hamster kidney cells using the full-length human chitotriosidase cDNA cloned in the pNUT vector (20). 1.5 mg of freeze-dried human chitinase was dissolved in 6 ml of 50 mM Tris/HCl, pH 8.7, and dialyzed against 1 liter of the same overnight at 4 °C. It was then spin-concentrated to 7.7 mg/ml. Vapor diffusion crystallization experiments were set up by mixing 0.5 μl of protein with an equal volume of 0.1 M Tris/HCl, pH 8.5, 30% PEG 4000. After 5 weeks of equilibration at room temperature, rod-shaped crystals grew to a size of 0.1 × 0.1 × 0.2 mm. Crystals were cryoprotected by a 10-s immersion in mother liquor with 15% PEG 2000 monomethylether and then frozen in a 100 K nitrogen gas stream. They belonged to space group $P4_32_12$ with cell parameters $a = b = 93.26$ Å, and $c = 89.80$ Å, with one protein molecule present per asymmetric unit.

Monoclinic chitotriosidase crystals were obtained at room temperature by mixing 5 μl of protein solution (10 mg/ml) with an equal volume of 0.1 M citrate buffer, pH 5.6, 24–27% PEG 3350, and 40% ethylene glycol. Crystals grew as plates to a size of 0.1 × 0.2 × 0.05 mm. The crystals were directly flash-frozen in a 100 K nitrogen stream. They belong to space group $P2_1$ with cell parameters $a = 45.17$ Å, $b = 47.29$ Å, $c = 84.73$ Å, and $\beta = 102.58°$ with one molecule in the asymmetric unit.

Crystals grown under slightly different conditions (0.1 M Tris/HCl, pH 9.0, 0.2 M Li_2SO_4, 32.5% PEG 4000, 20 °C) were used for soaks with allosamidin by the addition of 0.25 μl of a 50 mg/ml solution. The addition of the inhibitor resulted in severe cracking of the crystals. The soaked crystals were cryoprotected by a 10-s immersion in mother liquor with 10% glycerol and then frozen in a 100 K nitrogen gas stream.

Larger (1.0 × 0.1 × 0.1 mm) native tetragonal crystals of chitotriosidase could be obtained using a solution of 0.1 M citrate buffer, pH 5.6, 0.2 M ammonium acetate, 24–27% PEG 3350 as a precipitant. These crystals were soaked for 1 h at room temperature in 5 mM NAG_5 (N^I, N^{II}, N^{III}, N^{IV}, N^V-pentaacetylchitopentaose, Sigma), 0.1 M CAPS buffer, pH 10.6, 0.2 M ammonium acetate, 30% PEG 3350. Before soaking, the crystals were transferred from the mother liquor to the final solution by gradually increasing the pH.

Data Collection, Structure Solution, and Refinement—Data for the $P4_32_12$ crystals and allosamidin soaks were collected on beamlines ID14–1 and ID29 at the European Synchrotron Radiation Facility on Quantum-Q4 and Quantum-Q210 detectors, respectively. Data for the $P2_1$ crystals and $P4_32_12$ crystals soaked with NAG_5 were collected on an ENRAF-Nonius rotating anode with a MacScience DIP2030 image plate detector and at the ELETTRA synchrotron, Trieste, Italy on a MAR345 image plate detector, respectively (Table I). Data were processed with the HKL suite (21).

The native structure was solved in space group $P4_32_12$ by molecular replacement with AMoRe (22), using the structure of the lectin YM1 (23) as a search model, against 8–4-Å data. A clear solution was obtained ($r = 0.418$, correlation coefficient of 0.50). The model was then refined by iterative model building in O (24) and refinement in CNS (25) using a small set of reflections for calculation of R_{free} (Table I). A complete structure was obtained for residues Ala-22 to Leu-385, although residues 232–234 in a solvent-exposed loop could not be modeled due to disorder. The final model has an R-factor of 0.216 ($R_{free} = 0.262$). 98.7% of the residues are in allowed regions of the Ramachandran plot, and 1.3% are in "generously allowed" (three residues) or disallowed (one residue, Asp-278, in a less well defined loop) regions, according to the PROCHECK definitions (26). At a later stage, a second crystal form, in space group $P2_1$, was obtained from ethylene glycol solutions and was solved by molecular replacement using the $P4_32_12$ structure as a search model. Refinement and model building were performed as described above and resulted in a final model as outlined in Table I.

A complex of the chitotriosidase with NAG_2 was obtained by soaking crystals in $P4_32_12$ in NAG_5 (see above). Refinement revealed well ordered density in the active site corresponding to an *N*-acetylglucosamine dimer (see Fig. 1*B*), which was built and included in further refinement (see Table I).

Attempts to obtain a well defined chitotriosidase-allosamidin complex were hampered by cracking of allosamidin-soaked crystals, resulting in high mosaicity (varying from 0.9 to >2°) and rather large changes in unit cell dimensions (Table I). Here, we only use the unbiased $F_o - F_c$, ϕ_{calc} map at 2.7 Å (see Fig. 3*B*) after one round of refinement to confirm a model of the chitotriosidase-allosamidin complex constructed by superposition of the chitotriosidase with previously published chitinase-allosamidin complexes (27–29). All images were generated with PyMOL (www.pymol.org). Structural superpositions were performed with the MOTIF module in WHAT IF (30).

RESULTS AND DISCUSSION

Overall Structure and Interaction with Chitin—The structure of the 39-kDa form of human chitotriosidase was solved by molecular replacement and refined against 2.35-Å diffraction data to an R-factor of 0.216 ($R_{free} = 0.262$) in space group $P4_32_12$ with good stereochemistry (Table I, Fig. 1). The structure consists of two domains. The core domain has a $(\beta/\alpha)_8$ barrel as observed in the other family 18 chitinase structures for hevamine (31), chitinases A (ChiA) (17) and B (ChiB) (18)

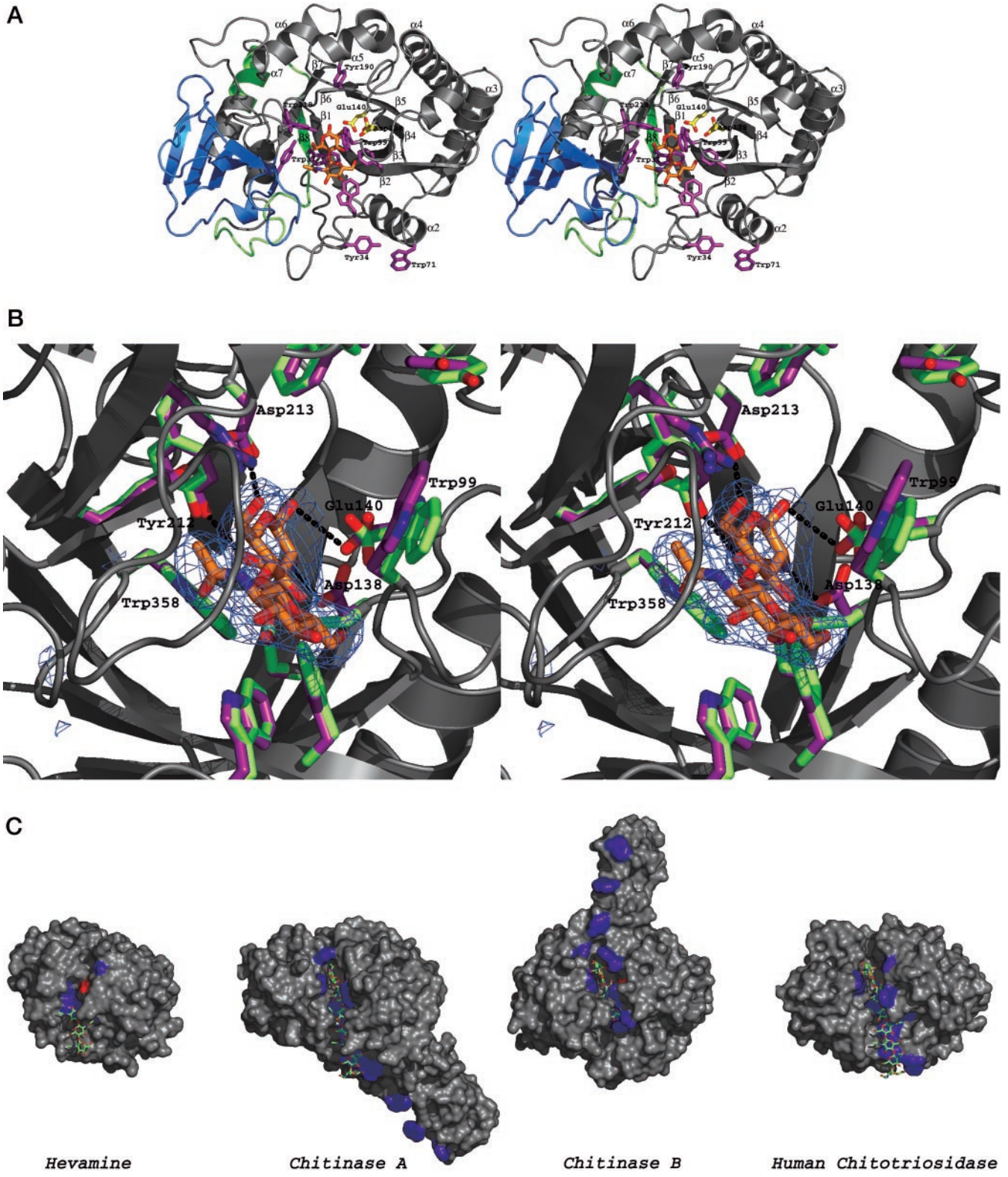

FIG. 1. **Overview of chitotriosidase structure and comparison with other chitinases.** *A*, stereo image of the final human chitotriosidase structure. The backbone is shown as a *gray ribbon*. The α/β domain is colored *blue*. Residues 344–372, which are deleted in the inherited mutated form of the enzyme, are colored *green*. Asp-136, Asp-138, and Glu-140 are shown as a sticks model with carbons colored *yellow*. Solvent-exposed aromatic side chains lining the active site cleft are shown as *purple sticks*. NAG_2, as seen in the complex (Table I), is shown in a sticks representation with *orange* carbon atoms. *B*, stereo image of the active site. The chitotriosidase backbone is shown as a *gray ribbon*. Solvent-exposed aromatics and residues interacting with NAG_2 are shown as *sticks* with carbons colored *green* for the apo structure and carbons colored *purple* for the chitotriosidase-NAG_2 complex. A simulated-annealing $F_o - F_c$, ϕ_{calc} map for NAG_2 as observed in the chitotriosidase-NAG_2 complex is shown in *blue*, contoured at 3σ. NAG_2 is shown in a *sticks representation* with *orange* carbon atoms. *C*, overall comparison with other chitinases. Molecular surfaces (calculated with PyMOL) are shown for currently known complexes of chitinases with chitooligosaccharides: hevamine with NAG_3 (31), ChiA with NAG_8 (32), ChiB with NAG_5 (29), and the human chitotriosidase with a model of NAG_9. The TIM barrel core of the enzymes is orientated as in *panel A*. The catalytic glutamic acid is colored *red*, and exposed aromatic side chains lining the active site cleft are colored *blue*. The chitooligosaccharides are shown as *sticks* with *green* carbons.

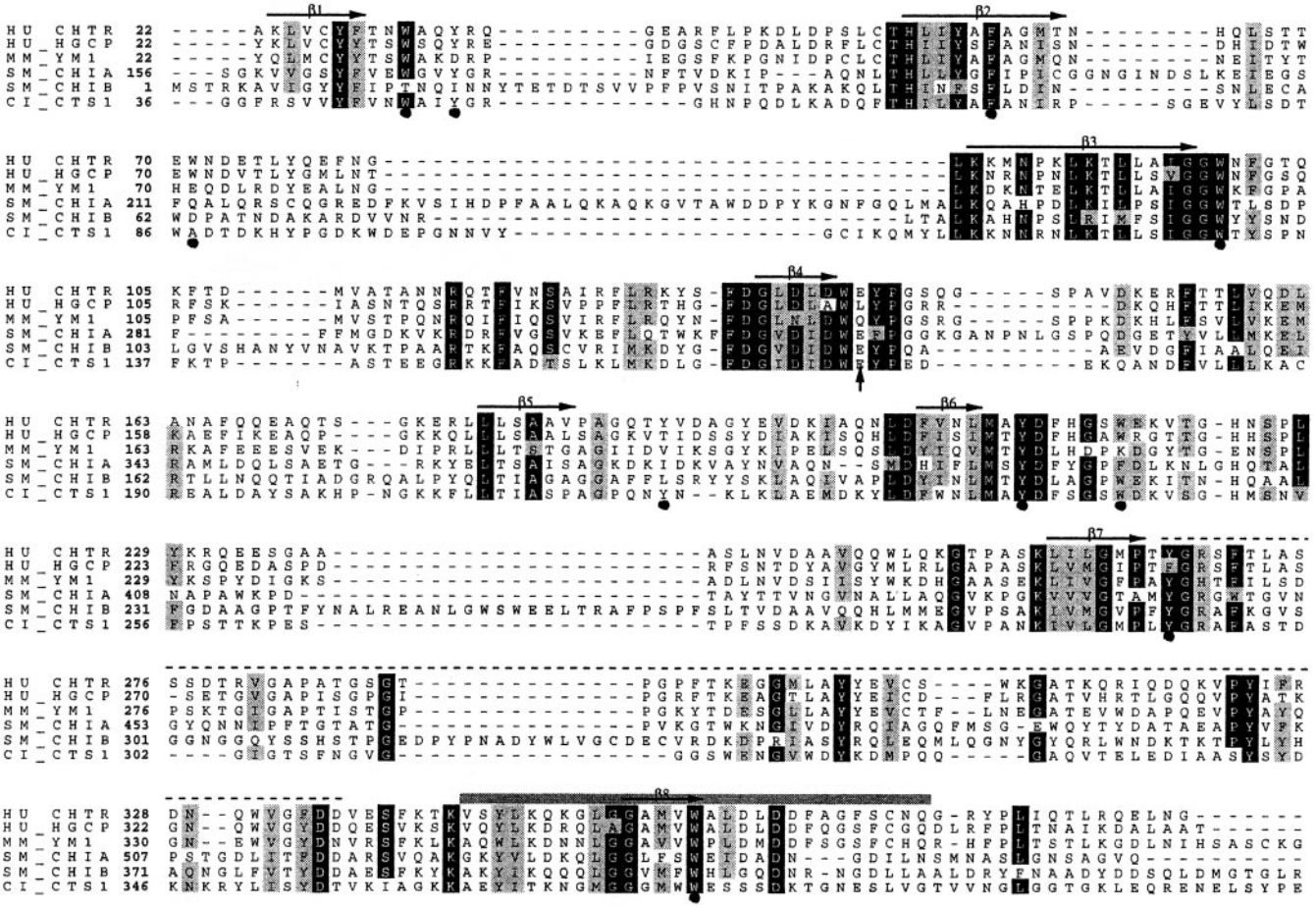

FIG. 2. **Sequence alignment of chitinases.** Structure-based sequence alignments between the human chitotriosidase (*HU_CHTR*) and other closely related structures (mouse YM1 (23) (*MM_YM1*), chitinase A (17) (*SM_CHIA*) and B (18) (*SM_CHIB*) from *S. marcescens*, and CTS1 from *C. immitis* (*CI_CTS1*) are shown. Also included is the sequence for HCgp-39 (37) (*HU_HCGP*), which was aligned with CLUSTAL-W (43). Conserved regions are *boxed*. The eight β-strands in the TIM barrel are indicated and *labeled*. The *long dotted line* represents the α/β domain (see also Fig. 1). The *gray bar* indicates the stretch of residues (344–372) deleted in the inherited inactive form of the chitotriosidase. Solvent-exposed aromatic residues lining the active site cleft are *labeled* with a *black dot*. The catalytic glutamic acid in the D*X*D*X*E motif (Glu-140 in the chitotriosidase) is indicated by an *arrow*.

from *S. marcescens*, and CTS1 from *Coccidioides immitis* (28), although helix α1 is missing (Fig. 1*A*). An additional α/β domain, composed of six antiparallel β-strands and one α-helix, is inserted in the loop between strand β7 and helix α7, which gives the active site a groove character (Fig. 1*C*). Like all other family 18 chitinases, the chitotriosidase has the D*X*D*X*E motif at the end of strand β4 with Glu-140 being the catalytic acid (Figs. 1*A* and 2). Two disulfide bridges were observed between Cys-26–Cys-51 and Cys-307–Cys-370, which are also present in the YM1 structure (23).

The native chitotriosidase structure was also refined using diffraction data from a second crystal form (space group $P2_1$, Table I). These crystals were obtained by adding 40% ethylene glycol to the precipitant solution. Ethylene glycol acts as an inhibitor of chitotriosidase, and the structure shows the presence of three molecules of ethylene glycol bound in the active site. One of them is hydrogen-bonded to Asp-138, which is essential for catalysis in chitinases (27, 29). This ethylene glycol molecule may inhibit the chitotriosidase by blocking the side chain of Asp-138 in the native position, preventing the binding of the substrate (attempts to bind NAG_2 failed). The $P4_32_12$ and $P2_1$ structures are essentially identical and superpose with a root mean squares deviation of 0.5 Å on C_a atoms. In further discussions below, the structure in space group $P4_32_12$ will be used when referring to the native human chitotriosidase structure.

Soaking experiments with chitooligosaccharides NAG_3, NAG_4, or NAG_5 were carried out at pH 10.6 to prevent acid-catalyzed hydrolysis of the substrate. Nevertheless, hydrolysis occurred, and the experiments consistently resulted in electron density maps where only an ordered *N*-acetylglucosamine dimer could be observed, lying in subsites −2 and −1 (Fig. 1*B*). The chitotriosidase structure shows little change upon NAG_2 binding. The most relevant is the side chain of Asp-138, which rotates toward the side chain of Glu-140, as seen in other studies with chitinases (29, 31–33) (Fig. 1*B*). Other side chains (Fig. 1*B*) undergo minor conformational changes, probably required to accommodate and stabilize the binding of the oligosaccharide. At 2.8-Å resolution (Table I), it is not possible to unambiguously distinguish a boat (as seen in the ChiA-NAG_8 (32) and ChiB-NAG_5 (29) complexes) from a chair (as seen in the hevamine-NAG_3 complex (31)) conformation in the −1 subsite. However, in our complex, the +1 subsite is not occupied, and we have therefore modeled the −1 sugar in the chair conformation.

Through superposition of the ChiB-NAG_5 complex (29) and the ChiA-NAG_8 complex (32) onto the chitotriosidase-NAG_2 structure, a model of a complex with NAG_9 can be produced (Fig. 1*C*), an approach used before to produce models of chitinase-ligand complexes (18, 28, 33). In the ChiB-NAG_5 complex, the oligosaccharide occupies subsites −2, −1, +1, +2, +3 (where the scissile glycosidic bond is located between sugars

−1 and +1 (34)), whereas in the ChiA-NAG_8 complex, subsites −6 to +2 are occupied (32). In the superpositions, the subsites −2 to +2 are occupied by the chitooligosaccharides from both the ChiA and ChiB complexes (the −2 to −1 subsites are also occupied by the chitotriosidase-NAG_2 complex), with the sugar atoms overlapping closely, to form a continuous NAG polymer from −6 to +3. In this model of the complex, the oxygen in the scissile glycosidic bond between the −1 and +1 sugars lies within hydrogen bonding distance (2.9 Å) of the carboxylic oxygen $O_{\epsilon 2}$ of the catalytic Glu-140. NAG_9 appears to fit the human chitotriosidase active site cleft without steric hindrance. Inspection of the active site lining reveals several solvent-exposed aromatic side chains that stack against the hydrophobic face of the sugars (Figs. 1 and 2). The pattern and conservation of these exposed aromatic residues is most reminiscent of that observed in ChiA with the conserved Trp-31 and Tyr-34 stabilizing the −6 non-reducing end of the bound chitin oligomer (Figs. 1 and 2). Although the pattern of exposed aromatic residues is most homologous to ChiA, the chitotriosidase has a more compact structure with several shorter loops (Figs. 1 and 2). The most striking difference, however, is that although ChiA has an N-terminal fibronectin type III domain, which is thought to be important for chitin binding (and has several exposed aromatic residues, Figs. 1 and 2) (17), the 39-kDa chitotriosidase form does not have such a domain (12). In contrast, an extra chitin binding domain is present in the 50-kDa form of the enzyme, but interestingly, this is located toward the C terminus, similar to what is observed in ChiB (18) (Fig. 1*C*). The sequence of the domain does not show homology to known structures, but similarities with the sequences of similar domains in nematodal and insect chitinases have been noted (13).

Although the human chitotriosidase has been established to be a fully active chitinase (11, 12), its precise substrate specificity has not been defined. The enzyme has been shown to hydrolyze 4-methylumbelliferyl β-D-chitooligosaccharides ($4MU\text{-}NAG_x$) (12) and to reduce various forms of polymeric chitin to dimers (12, 16), yet the experimental data do not exclusively classify it as either an endo- or exochitinase. Inspection of the structure provides some clues. ChiA and ChiB are both exochitinases and have a deep active site cleft, which is partially closed by overhanging loops, whereas the chitotriosidase cleft is more open (Fig. 1*C*). The ChiA/B active sites also appear to be blocked at opposite ends (at the reducing end for ChiA and at the non-reducing end for ChiB), which explains their synergism in the degradation of polymeric chitin (1). In contrast, the chitotriosidase active site cleft appears to be fully extended over one face of the enzyme, although narrowing somewhat at the far reducing end of the NAG_9 model (Fig. 1*C*). From a structural point of view, it is thus possible that the chitotriosidase is an endochitinase. This would be consistent with its proposed role as a defense protein against chitin-containing pathogens such as fungi and its ability to directly degrade chitin from *C. albicans* cell walls (12, 13, 16).

Structural Basis for Inherited Chitotriosidase Deficiency—As mentioned earlier, the chitotriosidase is a marker for Gaucher disease with plasma levels over 2 orders of magnitude elevated as compared with healthy control individuals (11). However, in the same study, it was also noted that about 1 in 20 individuals was completely deficient in active chitotriosidase (11). Detailed studies later revealed that this was an inherited genetic defect due to a 24-base pair duplication in exon 10 (15). This duplication generates a cryptic splice site, leading to an 87-nucleotide deletion with significantly decreased mRNA levels (15). Although the mRNA is translated normally, a completely inactive enzyme is produced with residues Val-344–Gln-372 missing. The chitotriosidase structure presented here allows us to understand why deletion of this region inactivates the enzyme. Figs. 1*A* and 2 show that residues 344–372 correspond to the C-terminal half of helix α7, the entire strand β8, and almost the entire β8-α8 loop. Deletion of these secondary structure elements could lead to misfolded, and therefore inactive, protein. More importantly perhaps, Trp-358, which lies at the end of strand β8, is completely conserved in all active family 18 chitinases (Fig. 2). Inspection of chitinase structures in complex with chitooligosaccharides (29, 32) shows that this tryptophan serves as an "anvil" onto which the −1 sugar is pressed, whereas specific hydrogen-bonds with other residues may force the sugar in the boat conformation required for the attack of the *N*-acetyl group on the anomeric carbon (29) (Fig. 1*A*). Thus, deletion of Trp-358 could in itself lead to a completely inactive enzyme.

Comparison with the Mammalian Lectins YM1 and HCgp-39—Apart from the human chitotriosidase, two other family 18 chitinase-like mammalian proteins have been described recently. YM1 and HCgp-39 both show a high degree of sequence similarity to family 18 chitinases (23, 35) (Fig. 2). The structure of YM1 has been determined by x-ray crystallography, revealing density for a single glucosamine in the active site (23). As was predicted from multiple sequence alignments (Fig. 2), two key residues in the active site were mutated (Asp-136 to Asn and Glu-140 to Gln), which renders the protein completely inactive as a chitinase. Binding experiments and crystallographic analysis further showed that YM1 does not interact with polymeric carbohydrates but rather with monomers (23, 36), although the YM1 structure did not reveal why the chitinase-like protein had lost its ability to interact with carbohydrate polymers. The human chitotriosidase structures presented here allow us to explain this loss of affinity (Fig. 3*A*). Apart from the elimination of catalytic activity through the mutations in the active site, there are several non-conservative substitutions in the chitin binding cleft. Tyr-24, near the non-reducing end of the substrate binding cleft, is replaced with an aspartic acid, whereas the nearby Trp-72 is replaced with a glutamic acid (Figs. 2 and 3*A*). On the other side of the cleft, Trp-218 is changed to a lysine, and Tyr-190 is replaced by the smaller valine. The trend in these mutations is that almost half of the exposed aromatic residues, discussed earlier and shown in Fig. 1, have been non-conservatively replaced, indeed in most cases with charged amino acids. Thus, although all the residues required for interaction with monomeric carbohydrates are still present in the core of the active site, the cleft-lining residues required for the binding of polymeric substrate have been removed. This explains the observed carbohydrate binding specificity (monomers only) for YM1 (36).

Similar to YM1, the human cartilage protein HCgp-39 has all the signs of an inactivated chitinase. Although its sequence suggests a family 18 chitinase-like structure, two key active site residues, the equivalents of Asp-138 and Glu-140 in the chitotriosidase, have been mutated to Ala and Leu, respectively, and HCgp-39 does not have detectable chitinase activity (37). Binding studies, however, have shown that unlike YM1, HCgp-39 binds chitin with high affinity and has therefore been proposed to be a chitin-specific lectin (35). A structure for HCcp-39 is not available. However, sequence alignment shows that unlike YM1, all of the solvent-exposed aromatics are conserved in HCgp-39 with the exception of Tyr-190, which is not a conserved residue in other chitinases either (Fig. 2). Thus, like the human chitotriosidase, the active site cleft of HCgp-39 would be lined with exposed aromatic residues and could support the binding of longer chitin oligomers.

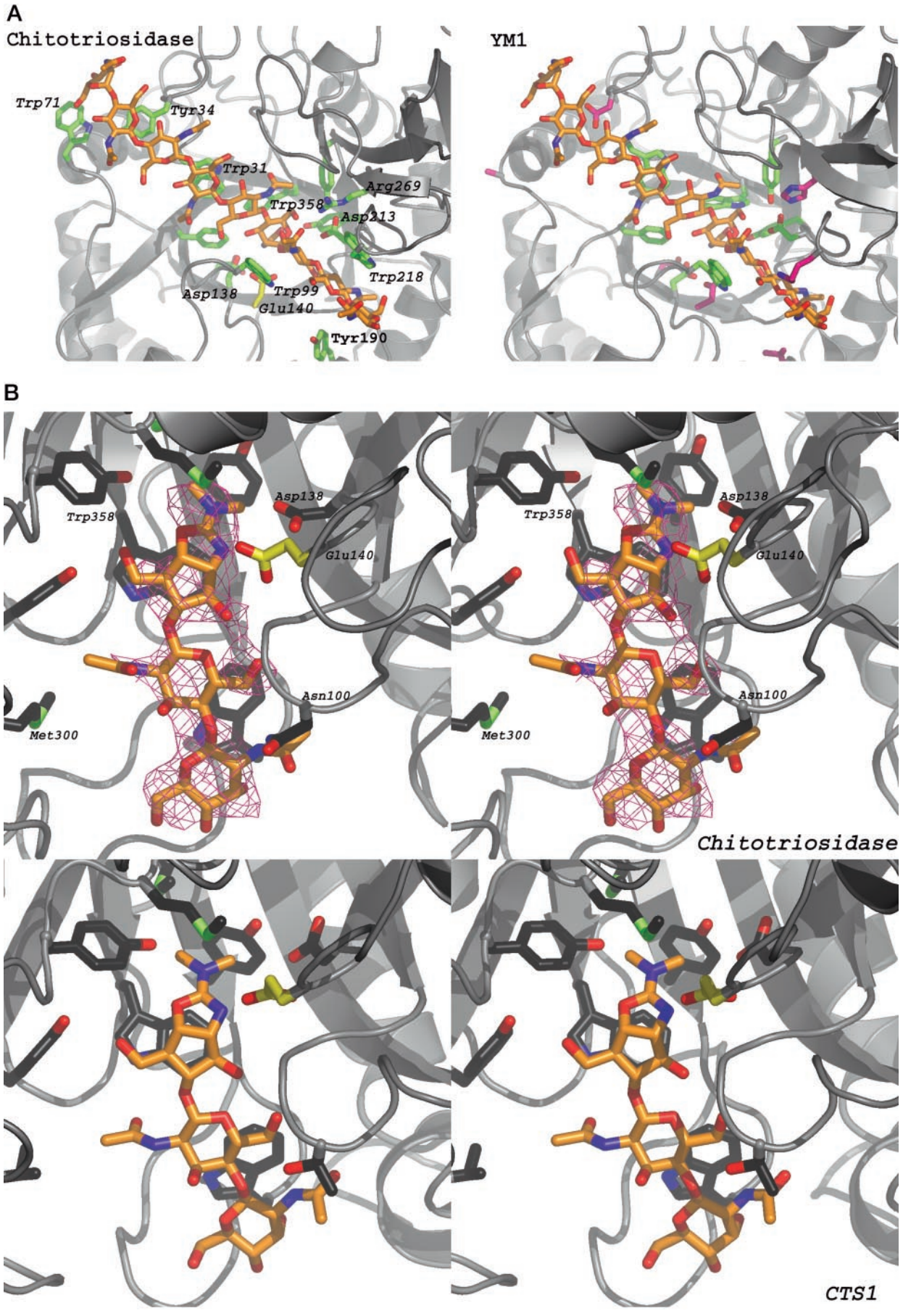

FIG. 3. **Comparison of active site details and interaction with allosamidin.** In *A*, the substrate binding pockets of the human chitotriosidase and YM1 are compared. Protein backbones are represented by a *gray ribbon*. A model of NAG_9, in equivalent position to that in Fig. 1, is

Implications for Selective Inhibitor Design—The most potent chitinase inhibitor currently known is allosamidin, a pseudotrisaccharide (consisting of two β(1,4)-linked *N*-acetyl allosamine sugars coupled to allosamizoline, Fig. 3*B*) isolated from *Streptomyces* (3, 38). All family 18 chitinases tested are inhibited by this molecule with K_i values in the nanomolar to micromolar range (39, 40); it inhibits the chitotriosidase with a K_i of 0.4 μM (16). Allosamidin has been shown to have a fungistatic effect by interfering with fungal cell separation (2, 9) and to act as a malaria transmission blocker as it strongly inhibits a *Plasmodium falciparum* chitinase required for insect invasion (6, 8). However, the recent implication that the human chitotriosidase, although not essential from a housekeeping point of view, may play a role in defense against pathogens (15, 19) suggests that a broad spectrum chitinase inhibitor might have negative side effects if administered to humans. Thus, if chitinase inhibitors, such as allosamidin, are further developed to enhance their fungicidal, insecticidal, and antimalarial potential, inhibition of the human chitotriosidase should be reduced to weak levels. We addressed this issue by soaking chitotriosidase crystals with allosamidin and positioning the inhibitor according to a 2.7-Å difference map (Fig. 3*B*). Comparison of this complex with the one obtained for the chitinase CTS1 from the fungal pathogen *C. immitis* (28), which is the causative agent of the respiratory disease known as San Joaquin Valley fever in the southern Americas, suggests a strategy for improving the efficacy of antifungal molecules. It is apparent that the overall shape of the active site in the −1 subsite is nearly identical for the chitotriosidase and CTS1 complexes with allosamidin and also for complexes of the inhibitor with hevamine (27) and ChiB (29). The allosamizoline moiety binds deep in the active site, interacting closely with, among others, Asp-138 and Trp-358, both completely conserved in family 18 chitinases (Fig. 2). Only few protein side chains interact with the allosamine sugars in the −2 and −3 positions (Fig. 3*B*), and it is also here that some differences are observed between the human and fungal enzymes. Asn-100, which hydrogen-bonds to the oxygen of the *N*-acetyl group on the −3 sugar, is replaced by the shorter threonine in the fungal enzyme (Fig. 3*B*). Met-300, which stacks against the methyl of the *N*-acetyl group on the −2 sugar, is a valine in the fungal enzyme, creating a small void (Fig. 3*B*). Thus, there appears to be scope for the development of allosamidin derivatives with differential specificity based on the changes around the −2 and −3 subsites. In this context, it is worth noticing that such derivatives have already been reported, although so far all changes in the allosamine sugars appear to reduce chitinase inhibition (39, 41, 42).

Conclusion—The structure of the human chitotriosidase and its complexes described here have provided further clues for understanding the possible functions of the protein and its closely related homologues, YM1 and HCgp-39. The structure reveals that a long cleft runs across one face of the protein and that this cleft is lined with solvent-exposed aromatic residues. This suggests the ability to bind long chitin polymers, and given the relatively open active site architecture, implies that chitotriosidase functions as an endochitinase rather than an exochitinase. The complex with NAG_2 followed by modeling of a longer chitooligosaccharide revealed that the active site would be able to accommodate longer chitin polymers, which agrees with its ability to degrade various forms of polymeric chitin. The human enzyme appears to have significant differences in the active site as compared with a chitinase from the pathogenic fungus *C. immitis*, which may be exploitable in the design of allosamidin derivatives or other inhibitors that show differential specificity toward human and pathogen chitinases.

Acknowledgments—We thank the European Synchrotron Radiation Facility, Grenoble, France, for the time at beamlines ID14–1 and ID29. We acknowledge the ELETTRA synchrotron for beam time and support. We are grateful to Graham Gooday for providing a sample of allosamidin. We also acknowledge Herma Renkema, Anneke Strijland, Wilma Donker, and Marri Verhoek for help in generating enough pure recombinant protein for these studies and Ulrike Van Der Wel for crystallographic contributions.

REFERENCES

1. Brurberg, M. B., Nes, I. F., and Eijsink, V. G. H. (1996) *Microbiology* **142,** 1581–1589
2. Kuranda, M. J., and Robbins, P. W. (1991) *J. Biol. Chem.* **266,** 19758–19767
3. Sakuda, S., Isogai, A., Matsumoto, S., and Suzuki, A. (1987) *J. Antibiot. (Tokyo)* **40,** 296–300
4. Flach, J., Pilet, P. E., and Jolles, P. (1992) *Experientia (Basel)* **48,** 701–716
5. Hawtin, R. E., Arnold, K., Ayres, M. D., Zanotto, P. M. D., Howard, S. C., Gooday, G. W., Chappell, L. H., Kitts, P. A., King, L. A., and Possee, R. D. (1995) *Virology* **212,** 673–685
6. Vinetz, J. M., Dave, S. K., Specht, C. A., Brameld, K. A., Xu, B., Hayward, R., and Fidock, D. A. (1999) *Proc. Natl. Acad. Sci. U. S. A.* **96,** 14061–14066
7. Izumida, H., Imamura, N., and Sano, H. (1996) *J. Antibiot. (Tokyo)* **49,** 76–80
8. Vinetz, J. M., Valenzuela, J. G., Specht, C. A., Aravind, L., Langer, R. C., Ribeiro, J. M. C., and Kaslow, D. C. (2000) *J. Biol. Chem.* **275,** 10331–10341
9. Sami, L., Pusztahelyi, T., Emri, T., Varecza, Z., Fekete, A., Grallert, A., Karanyi, Z., Kiss, L., and Pocsi, I. (2001) *J. Gen. Appl. Microbiol.* **47,** 201–211
10. Barranger, J. A., and Ginns, E. I. (1988) in *Glucosylceramide Lipidoses: Gaucher's Disease,* (Scriver, C. R., Beaudet, A. L., Sly, W. S., and Valle, D., eds), pp. 1677–1698, McGraw-Hill Inc., New York
11. Hollak, C. E. M., van Weely, S., van Oers, M. H. J., and Aerts, J. M. F. G. (1994) *J. Clin. Invest.* **93,** 1288–1292
12. Renkema, G. H., Boot, R. G., Muijsers, A. O., Donker-Koopman, W. E., and Aerts, J. M. F. G. (1995) *J. Biol. Chem.* **270,** 2198–2202
13. Boot, R. G., Renkema, G. H., Strijland, A., van Zonneveld, A. J., and Aerts, J. M. F. G. (1995) *J. Biol. Chem.* **270,** 26252–26256
14. Renkema, G. H., Boot, R. G., Strijland, A., Donker-Koopman, W. E., van den Berg, M., Muijsers, A. O., and Aerts, J. M. F. G. (1997) *Eur. J. Biochem.* **244,** 279–285
15. Boot, R. G., Renkema, G. H., Verhoek, M., Strijland, A., Bliek, J., de Meulemeester, T. M. A. M. O., Mannens, M. M. A. M., and Aerts, J. M. F. G. (1998) *J. Biol. Chem.* **273,** 25680–25685
16. Boot, R. G., Blommaart, E. F. C., Swart, E., van der Vlugt, K. G., Bijl, N., Moe, C., Place, A., and Aerts, J. M. F. G. (2001) *J. Biol. Chem.* **276,** 6770–6778
17. Perrakis, A., Tews, I., Dauter, Z., Oppenheim, A. B., Chet, I., Wilson, K. S., and Vorgias, C. E. (1994) *Structure* **2,** 1169–1180
18. van Aalten, D. M. F., Synstad, B., Brurberg, M. B., Hough, E., Riise, B. W., Eijsink, V. G. H., and Wierenga, R. K. (2000) *Proc. Natl. Acad. Sci. U. S. A.* **97,** 5842–5847
19. Choi, E. H., Zimmerman, P. A., Foster, C. B., Zhu, S., Kumaraswami, V., Nutman, T. B., and Chanock, S. J. (2001) *Genes Immun.* **2,** 248–253
20. Funk, W. D., MacGillivray, R. T. A., Mason, A. B., Brown, S. A., and Woodworth, R. C. (1990) *Biochemistry* **29,** 1654–1660
21. Otwinowski, Z., and Minor, W. (1997) *Methods Enzymol.* **276,** 307–326
22. Navaza, J. (1994) *Acta Crystallogr. Sect. A,* **50**, 157–163
23. Sun, Y. J., Chang, N. C. A., Hung, S. I., Chang, A. C., Chou, C. C., and Hsiao, C. D. (2001) *J. Biol. Chem.* **276,** 17507–17514
24. Jones, T. A., Zou, J. Y., Cowan, S. W., and Kjeldgaard, M. (1991) *Acta Crystallogr. Sect. A,* **47**, 110–119
25. Brünger, A. T., Adams, P. D., Clore, G. M., Gros, P., Grosse-Kunstleve, R. W., Jiang, J.-S., Kuszewski, J., Nilges, M., Pannu, N. S., Read, R. J., Rice, L. M., Simonson, T., and Warren, G. L. (1998) *Acta Crystallogr. Sect. D Biol. Crystallogr.,* **54**, 905–921
26. Laskowski, R. A., McArthur, M. W., Moss, D. S., and Thornton, J. M. (1993) *J. Appl. Crystallogr.* **26,** 283–291
27. Terwisscha van Scheltinga, A. C., Armand, S., Kalk, K. H., Isogai, A., Henrissat, B., and Dijkstra, B. W. (1995) *Biochemistry* **34,** 15619–15623
28. Hollis, T., Mozingo, A. F., Bortone, K., Ernst, S., Cox, R., and Robertus, J. D. (2000) *Protein Sci.* **9,** 544–551
29. van Aalten, D. M. F., Komander, D., Synstad, B., Gåseidnes, S., Peter, M. G.,

shown as a *sticks drawing* with *orange* carbons. Side chains in the active site cleft are shown as *sticks* with *green* carbons, except for the catalytic glutamic acid, which is shown with *yellow* carbons. For YM1, non-conserved residues are shown with *magenta* carbons. In *B*, the interaction with allosamidin is compared for the chitotriosidase complex described here and the published *C. immitis* CTS1 chitinase complex (28). For both complexes, the enzyme backbone is shown as a *gray ribbons* model in stereo, and allosamidin is shown in a *sticks representation* with carbons colored *orange*. For the chitotriosidase, side chains contacting the inhibitor (defined as <sum of van der Waals radii + 0.5 Å) are shown as *sticks* with *black* carbons. An unbiased $F_o - F_c$, ϕ_{calc} map (*i.e.* before the inclusion of any allosamidin model) is shown in *magenta*, contoured at 2.25 σ. For the CTS1-allosamidin complex, equivalent side chains are shown.

and Eijsink, V. G. H. (2001) *Proc. Natl. Acad. Sci. U. S. A.* **98,** 8979–8984
30. Vriend, G. (1990) *J. Mol. Graph.* **8,** 52–56
31. Terwisscha van Scheltinga, A. C., Kalk, K. H., Beintema, J. J., and Dijkstra, B. W. (1994) *Structure* **2,** 1181–1189
32. Papanikolau, Y., Prag, G., Tavlas, G., Vorgias, C. E., Oppenheim, A. B., and Petratos, K. (2001) *Biochemistry* **40,** 11338–11343
33. Tews, I., Terwisscha van Scheltinga, A. C., Perrakis, A., Wilson, K. S., and Dijkstra, B. W. (1997) *J. Am. Chem. Soc.* **119,** 7954–7959
34. Davies, G. J., Wilson, K. S., and Henrissat, B. (1997) *Biochem. J.* **321,** 557–559
35. Renkema, G. H., Boot, R. G., Au, F. L., Donker-Koopman, W. E., Strijland, A., Muijsers, A. O., Hrebicek, M., and Aerts, J. M. F. G. (1998) *Eur. J. Biochem.* **251,** 504–509
36. Chang, N. C. A., Hung, S. I., Hwa, K. Y., Kato, I., Chen, J. E., Liu, C. H., and Chang, A. C. (2001) *J. Biol. Chem.* **276,** 17497–17506
37. Hakala, B. E., White, C., and Recklies, A. D. (1993) *J. Biol. Chem.* **268,** 25803–25810
38. Sakuda, S., Isogai, A., Matsumoto, S., Suzuki, A., and Koseki, K. (1986) *Tetrahedron Lett.* **27,** 2475–2478
39. Spindler-Barth, M., Blattner, R., Vorgias, C. E., and Spindler, K. D. (1998) *Pestic. Sci.* **52,** 47–52
40. Bokma, E., Barends, T., Terwisscha van Scheltinga, A. C., Dijkstra, B. W., and Beintema, J. J. (2000) *FEBS Lett.* **478,** 119–122
41. Nishimoto, Y., Sakuda, S., Takayama, S., and Yamada, Y. (1991) *J. Antibiot.* (*Tokyo*) **44,** 716–722
42. Blattner, R., Gerard, P. J., and Spindler-Barth, M. (1997) *Pestic. Sci.* **50,** 312–318
43. Thompson, J. D., Higgins, D. G., and Gibson, T. J. (1994) *Nucleic Acids Res.* **22,** 4673–4680

Structure of Human Chitotriosidase: IMPLICATIONS FOR SPECIFIC INHIBITOR DESIGN AND FUNCTION OF MAMMALIAN CHITINASE-LIKE LECTINS

Fabrizia Fusetti, Holger von Moeller, Douglas Houston, Henriëtte J. Rozeboom, Bauke W. Dijkstra, Rolf G. Boot, Johannes M. F. G. Aerts and Daan M. F. van Aalten

J. Biol. Chem. 2002, 277:25537-25544.
doi: 10.1074/jbc.M201636200 originally published online April 17, 2002
